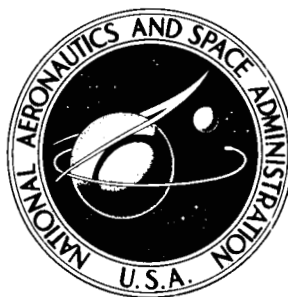NASA TN D-5503

CASE FILE COPY

ELECTROCHEMICAL BEHAVIOR OF THE ALUMINUM ELECTRODE IN MOLTEN SALT ELECTROLYTES

by Betty S. Del Duca

Lewis Research Center

Cleveland, Ohio

1. Report No. NASA TN D-5503	2. Government Accession No.	3. Recipient's Catalog No.
4. Title and Subtitle ELECTROCHEMICAL BEHAVIOR OF THE ALUMINUM ELECTRODE IN MOLTEN SALT ELECTROLYTES		5. Report Date October 1969
		6. Performing Organization Code
7. Author(s) Betty S. Del Duca		8. Performing Organization Report No. E-5053
9. Performing Organization Name and Address Lewis Research Center National Aeronautics and Space Administration Cleveland, Ohio 44135		10. Work Unit No. 120-34
		11. Contract or Grant No.
		13. Type of Report and Period Covered Technical Note
12. Sponsoring Agency Name and Address National Aeronautics and Space Administration Washington, D.C. 20546		
		14. Sponsoring Agency Code

15. Supplementary Notes

16. Abstract

The kinetics for dissolution and deposition of solid aluminum in molten $AlCl_3 \cdot NaCl$ and $AlCl_3 \cdot (LiCl\text{-}KCl)_{eut}$ electrolytes were studied by means of galvanostatic and potentiostatic techniques over a temperature range of 175° to 313° C (448 to 586 K). The apparent exchange currents varied from 1 to 56 mA/cm^2. Surface diffusion was found to be the rate-determining step at low overpotentials, and charge transfer the rate-determining step at high overpotentials. The most probable anodic rate-determining step was found to be $Al \rightarrow Al^+ + e^-$; the most probable cathodic rate-determining step was $Al^{+++} + e^- \rightarrow Al^{++}$ in $AlCl_3\text{-}(LiCl\text{-}KCl)_{eut}$ electrolyte and $Al^{++} + e^- \rightarrow Al^+$ in $AlCl_3 \cdot NaCl$ electrolyte. Current efficiencies for dissolution were close to 100 percent.

17. Key Words (Suggested by Author(s)) Aluminum electrodes Molten salt electrolytes	18. Distribution Statement Unclassified - unlimited

19. Security Classif. (of this report) Unclassified	20. Security Classif. (of this page) Unclassified	21. No. of Pages 30	22. Price* $3.00

ELECTROCHEMICAL BEHAVIOR OF THE ALUMINUM
ELECTRODE IN MOLTEN SALT ELECTROLYTES

by Betty S. Del Duca

Lewis Research Center

SUMMARY

Aluminum is a lightweight, inexpensive material of interest for use as a negative electrode in secondary batteries, particularly with low melting aluminum chloride $(AlCl_3)$ - alkali chloride electrolytes. The electrochemical kinetics for the dissolution and deposition of solid aluminum in high-purity $AlCl_3$-$(LiCl$-$KCl)_{eut}$ and $AlCl_3 \cdot NaCl$ electrolytes were studied by using transient and steady-state galvanostatic and potentiostatic techniques. Measurements were made over a temperature range of 175° to 313° C (448 to 586 K) and a potential range of 0 to 300 millivolts anodic and cathodic.

By consideration of (1) the rise time of the overpotential η following a constant current step, (2) the shape of Tafel (overpotential against log current density) plots at low overpotentials, and (3) the linearity of current-overpotential curves at $\eta \ll RT/nF$, the reaction was found to be controlled by the diffusion of surface adsorbed cations in the potential ranges of 0 to 70 millivolts anodic and 0 to 170 millivolts cathodic. The equilibrium concentration of the adion in $AlCl_3 \cdot NaCl$ electrolyte was calculated to be 0.17×10^{-10} moles per square centimeter at 220° C (493 K) and the equilibrium surface diffusion velocity to be about 0.0043 ampere per square centimeter.

The rate-determining steps at higher potentials were found to be charge-transfer processes, based on the linearity of Tafel plots and the absence of diffusion control in the electrolyte. Apparent exchange currents varied from 2 to 56 milliamperes per square centimeter for $AlCl_3$-$(LiCl$-$KCl)_{eut}$ electrolytes and 1 to 10 milliamperes per square centimeter for $LiCl \cdot NaCl$ electrolytes. The slopes of the Tafel plots were used to show that the most probable anodic rate-determining step is $Al \rightarrow Al^+ + e^-$. The most probable cathodic rate-determining step is $Al^{+++} + e^- \rightarrow Al^{++}$ for $AlCl_3$-$(LiCl$-$KCl)_{eut}$ electrolytes and $Al^{++} + e^- \rightarrow Al^+$ for $AlCl_3 \cdot NaCl$ electrolytes.

Current efficiencies were determined by weight loss - gain experiments. The anodic efficiency was close to 100 percent for currents of 0.3 to 0.5 milliampere per square centimeter. Cathodic current densities above 10 milliamperes per square centi-

·meter produced a dendritic deposit.

INTRODUCTION

In the search for high-energy-density, rechargeable anodes for electrochemical power applications, aluminum appears to be a promising choice for several reasons. It has low equivalent weight, is readily available and inexpensive, and exhibits a high potential. Its use in aqueous systems is hampered by passivity in most electrolytes or by corrosion in nonpassivating electrolytes. Zaromb (ref. 1) has discussed its application in aqueous primary and chemically rechargeable cells, but electrochemical recharging is not possible from aqueous solutions. Aluminum can be electrodeposited from non-aqueous organic solutions (ref. 2) and from molten salts (ref. 3). Molten-salt systems appear most promising in a secondary battery application for three main reasons: (1) aluminum can be deposited from the electrolyte, (2) the alkali halide - aluminum chloride mixtures have relatively low melting temperatures, and (3) these melts have electrical conductivities in the range of 0.1 to 0.2 ohm^{-1} centimeter^{-1} (ref. 4), which is one to two orders of magnitude higher than those of the typical organic electrolytes.

Few electrochemical investigations of aluminum in molten salts have been described. The aluminum-cryolite system has been studied extensively (refs. 3, 5, and 6), but the melting point of this electrolyte is greater than 725° C (1000 K), which is unattractive for battery applications. Laitinen and Liu (ref. 7) have measured the potential of aluminum electrodes in the lithium chloride - potassium chloride (LiCl-KCl) eutectic relative to the Pt/Pt^{++} reference electrode. They place aluminum fourth, after lithium, magnesium, and manganese, in the electromotive force series. They found the overall reaction valence change to be close to 3.0. Piontelli and Sternheim (ref. 8) studied the current-potential behavior of aluminum electrodes in AlCl$_3$-NaCl at 200° C (473 K). The contribution of charge transfer to the measured overvoltage was shown to be negligible for both the anodic and cathodic reactions. More recently, King, Brown, and Frayer (ref. 9) in a preliminary study found no measurable charge transfer or diffusion polarization at current densities as high as 1 to 2 amperes per square centimeter in 40 mole percent NaCl - 60 mole percent AlCl$_3$.

The present work was undertaken to explore the electrochemical properties of aluminum in a variety of molten-salt solutions. Current-potential (polarization) curves, current efficiencies, and the nature of the cathodic deposit were examined. The polarization measurements were carried out on solid aluminum electrodes using transient and steady-state galvanostatic (constant current) and potentiostatic (constant potential) techniques. Tafel plots (overpotential against log i) were constructed and interpreted in terms of the rate-determining steps for the anodic dissolution and cathodic deposition reaction. The electrolytes studied were mixtures of aluminum chloride with alkali ha-

2

lides melting between 110° and 160° C (383 and 533 K).

EXPERIMENTAL PROCEDURE

Preparation of Melts

The lithium chloride - potassium chloride eutectic (41 mole percent LiCl - 59 mole percent KCl), hereinafter referred to as $(LiCl-KCl)_{eut}$, and mixtures of $AlCl_3$ in the eutectic were obtained commercially in evacuated sealed vials. The former was certified as having a residual current not larger than 1.6 microamperes at 2 volts and 410° C. The $AlCl_3$-NaCl mixtures were prepared at this laboratory from reagent-grade chemicals which were dried at 110° C.

All samples containing $AlCl_3$ even though specified as "high purity" were found to be contaminated with organic materials which pyrolyzed upon heating. The techniques used for purification varied depending on the concentration of aluminum chloride in the melt. The electrolyte purification, cell construction, and preparation of the $AlCl_3$-NaCl melts were done by Dr. Jacob Greenberg.

Equimolar mixtures $[AlCl_3 \cdot NaCl, AlCl_3 \cdot (LiCl-KCl)_{eut}]$. - Melts in which $AlCl_3$ and alkali chloride were present in equal amounts had low vapor pressures (<1 torr at 500° C). The organic impurities were removed by thermal decomposition. The mixture was heated in pyrex tubes under flowing nitrogen. Vigorous bubbling began at 520° C and continued for 1 to several hours. When bubbling ceased, a clear straw-colored melt was obtained with a black carbon residue. The yellow coloration was attributed to the presence of small amounts of an oxychloride (private communication from Anderson Physics Laboratories, Inc.) and was removed by introducing an aluminum wire into the melt. A black precipitate formed on the wire and the melt became water-white. Presumably the oxychloride reacts with metallic aluminum to form soluble aluminum chloride and insoluble aluminum oxide. The yellow coloration could be recreated by bubbling oxygen into the purified melt and could be removed again by the aluminum treatment. Other investigators have reported a yellow coloration due to iron impurities which were removed by sublimation (ref. 10) or by treatment with metallic aluminum (ref. 11). No iron was detected by spectrographic analysis (sensitivity, 0.03 ppm) of the melts used in the present work.

After purification, the clear melt was transferred under inert conditions to a dry, heated electrochemical cell, which was evacuated to 1 torr and sealed off.

Mixtures containing more than 50 mole percent $AlCl_3$. - It was not possible to thermally decompose organic material present in these solutions because of the high partial vapor pressure of aluminum chloride over the melts. The organic material and oxychlo-

·ride were removed by heating at 250° C in the presence of metallic aluminum for several days. The organics slowly distilled into cold traps in an adjacent sidearm. A second · sidearm was kept heated and used to transfer the purified melt into the attached electrochemical cell by tipping the apparatus. The melt was allowed to freeze, and the cell was sealed under reduced pressure.

Mixtures containing less than 50 mole percent $AlCl_3$. - Three methods were used in an attempt to prepare melts of less than 50 mole percent $AlCl_3$. In one case, aluminum chloride was distilled into molten $(LiCl-KCl)_{eut}$ and, in a second method, molten $AlCl_3 \cdot (LiCl-KCl)_{eut}$ was added to molten $(LiCl-KCl)_{eut}$. In both cases, an immiscible two-phase system resulted. Apparently, the $AlCl_3$-containing liquid floated on top of the LiCl-KCl eutectic. Heating to 550° C (823 K) did not produce a single liquid phase. The third method involved anodic dissolution of aluminum electrodes, using a graphite counter electrode, into $(LiCl-KCl)_{eut}$ and was also unsuccessful. A black precipitate formed in amounts proportional to the electrolysis time. X-ray analysis of the precipitate gave strong patterns of aluminum, traces of magnesium oxide, and an unidentifiable material not present in the ASTM file but similar in structure to asbestos. Spectrographic analysis of the melt revealed only trace amounts of aluminum at the longest electrolysis times. Numerous attempts at various current densities produced the same black precipitate. It is important to note that this problem was never encountered when aluminum was anodically dissolved in melts containing $AlCl_3$. In fact, good anodic current efficiencies for aluminum dissolution were obtained (see section Current Efficiencies).

TABLE I. - RANGE OF EXPERIMENTAL VARIABLES

Electrolyte composition, mole percent	Temperature		Current density, mA/cm^2
	°C	K	
50 $AlCl_3$ - 50 $(LiCl-KCl)_{eut}$	202 213	475 486	0 to 25 anodic 0 to 100 cathodic
67 $AlCl_3$ - 33 $(LiCl-KCl)_{eut}$	187	460	0 to 30 anodic 0 to 100 cathodic
75 $AlCl_3$ - 25 $(LiCl-KCl)_{eut}$	235 265	508 538	0 to 300 anodic 0 to 300 cathodic
50 $AlCl_3$ - 50 NaCl	175 197 253 260 304 313	448 470 526 533 577 586	0 to 20 anodic 0 to 30 cathodic

4

At the conclusion of the electrochemical experiments, all the melts were analyzed by standard techniques. In all cases, compositions were within ±5 percent of the values listed in table I.

Electrochemical Cell

The cell used to obtain the electrochemical data is shown in figure 1. Forty-mil (1.02-mm) wires of 99.99 percent aluminum were washed with acetone to remove grease and mechanically connected to tungsten rods to form working, counter, and reference
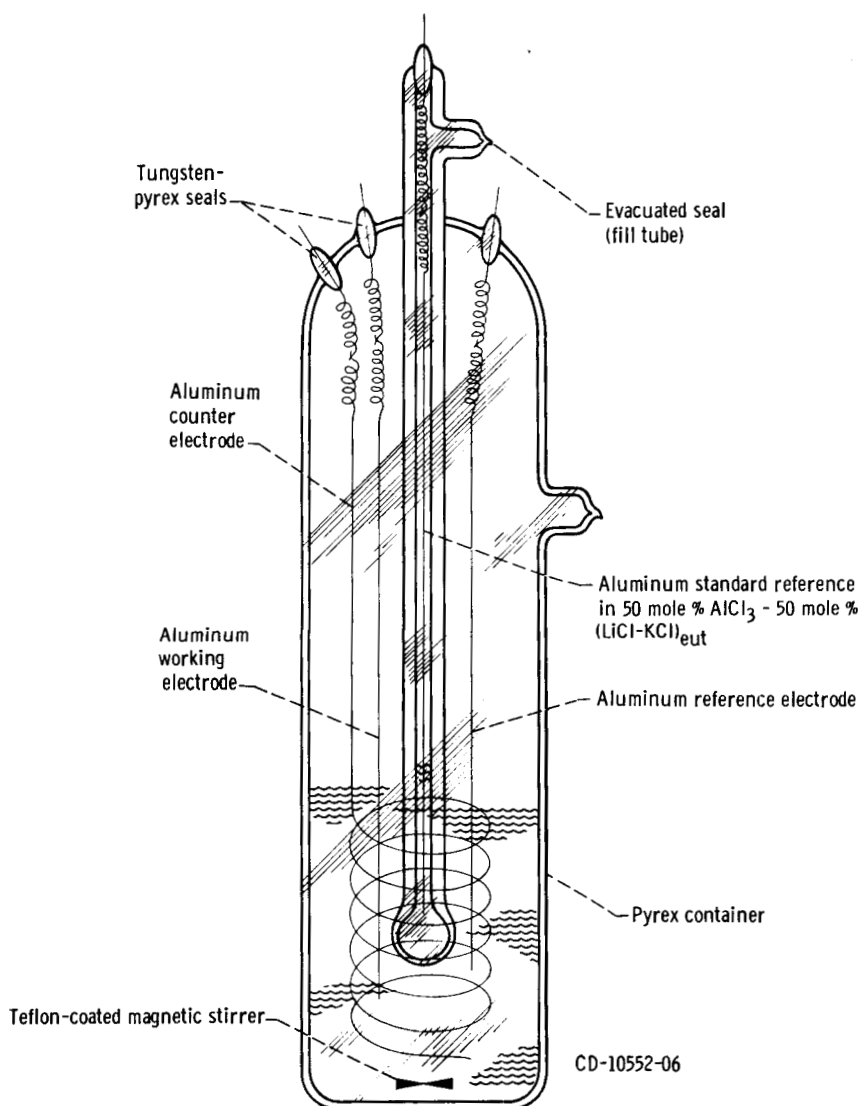
Tungsten-pyrex seals

Evacuated seal (fill tube)

Aluminum counter electrode

Aluminum standard reference in 50 mole % $AlCl_3$ - 50 mole % $(LiCl-KCl)_{eut}$

Aluminum working electrode

Aluminum reference electrode

Pyrex container

Teflon-coated magnetic stirrer

CD-10552-06

Figure 1. - Electrochemical cell.

electrodes. Aluminum wire was used as a reference for the galvanostatic and potentio-static measurements. This gives an open-circuit voltage of zero, and the applied or resultant voltage is thus the overpotential on the working electrode.

Equilibrium potentials of the aluminum anode in the various electrolytes were measured relative to a "standard" reference electrode of aluminum wire in $AlCl_3 \cdot$ $(LiCl-KCl)_{eut}$. The reference electrode was made by sealing a piece of 8-millimeter pyrex tubing so as to leave a micro-opening at the bottom. The micro-opening assures electrolytic contact while minimizing loss of electrolyte from the reference compartment. The micro-opening was formed by allowing the tube to almost close upon heating. Only those tubes with a resistance of 1000 to 2000 ohms between an inner and outer aluminum electrode immersed in a saturated aqueous solution of sodium chloride were used. The standard reference electrode was then completed by filling with $AlCl_3 \cdot (LiCl-KCl)_{eut}$, sealing in a tungsten lead with an aluminum wire extension, evacuating to 1 torr and sealing off.

The cell temperature was controlled within $\pm 5^{\circ}$ C by means of a thermostated oil bath. A magnetic stirrer was used to agitate the electrolyte when this was desired.

Instrumentation

Galvanostatic measurements. - Galvanostatic techniques were used to determine the ohmic (IR) drop of the solution and electrodes in the conventional manner (fig. 2) and to obtain transient overpotential time data (fig. 3). A potentiostat with a rise time specification of 1 to 3 microseconds (± 60 V ± 300 mA) was used to apply steady anodic and cathodic currents to the electrode. (Rise times of less than 10 μ sec were obtained with this circuit applied to the aqueous Cu/Cu^{++} system. This indicates that the performance of the instrumentation is acceptable.) The block diagram is shown in figure 4. The control amplifier inputs (+, -) and output should be identified with the potentiostat terminals: "control potential," "reference electrode," and "counter electrode," respectively. A mercury-relay pulse generator of conventional design supplied a potential pulse of selected length and magnitude to the control circuit of the potentiostat. This, in turn, controlled the potential across a precision resistor of 100 ohms, thereby establishing a constant current through the cell. The pulse was triggered by the gate output of a Tektronix 535A oscilloscope. The potential transients were displayed on the oscilloscope with a type D differential amplifier and photographed (see figs. 2 and 3 for typical traces).

Potentiostatic measurements. - Steady-state current-potential relations were determined by potentiostatically controlling the overpotential and observing the current on the potentiostat milliammeter at times of approximately 30 seconds. This time was chosen for two reasons: (1) at all current densities applied, the potential had reached a steady value within this time period; and (2) it was relatively short so that very little electroly-
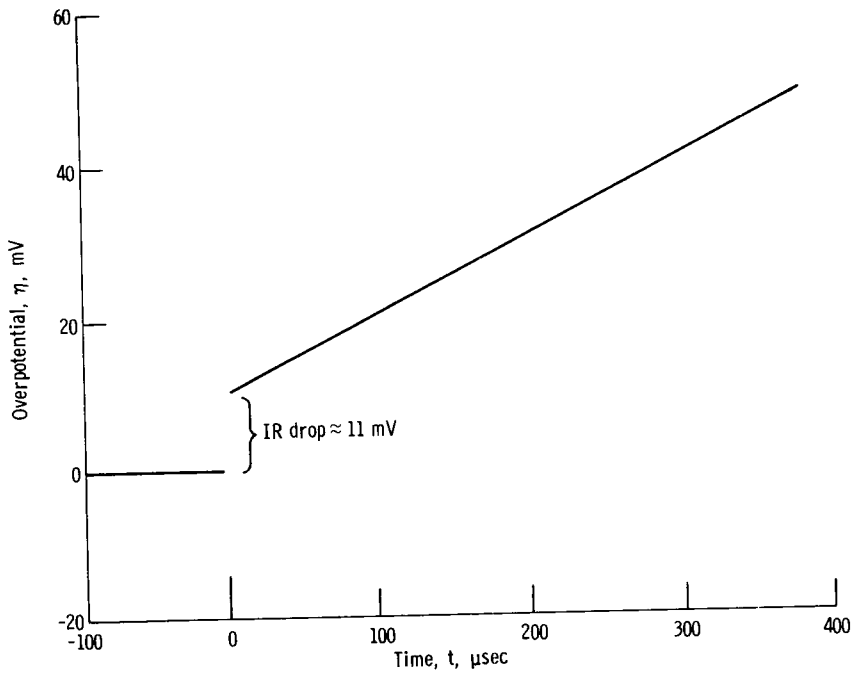
6

Figure 2. - Overpotential-time transient. Aluminum anode in 50 mole percent AlCl$_3$ - 50 mole percent NaCl; current density, 40 milliamperes per square centimeter.
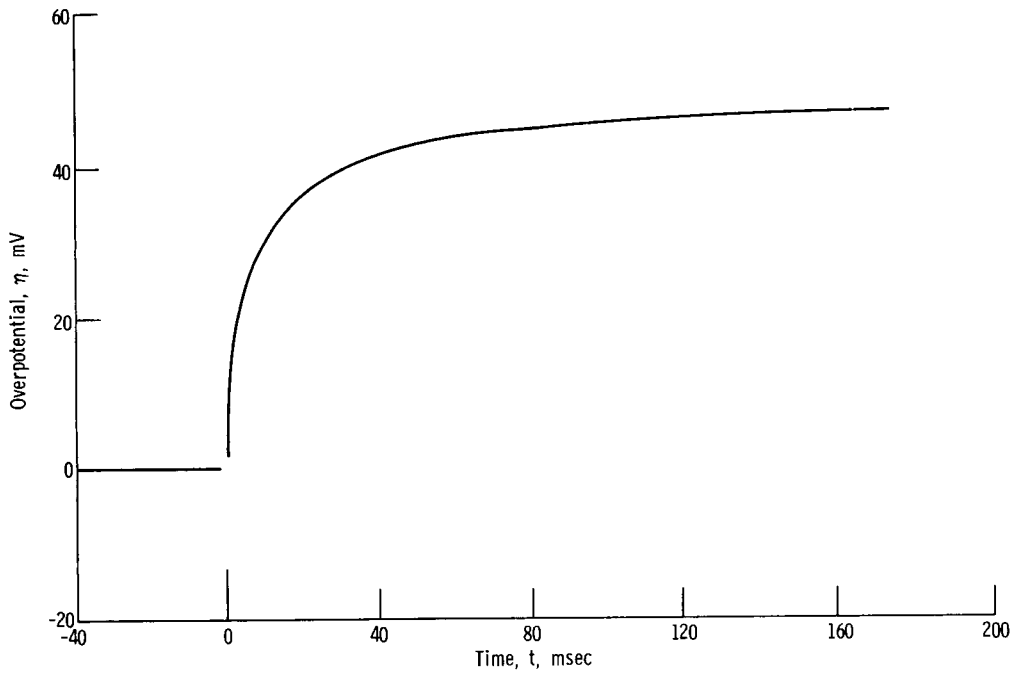

Figure 3. - Transient overpotential-time data. Aluminum anode in 50 mole percent AlCl$_3$ - 50 mole percent NaCl; current density, 9.1 milliamperes per square centimeter.
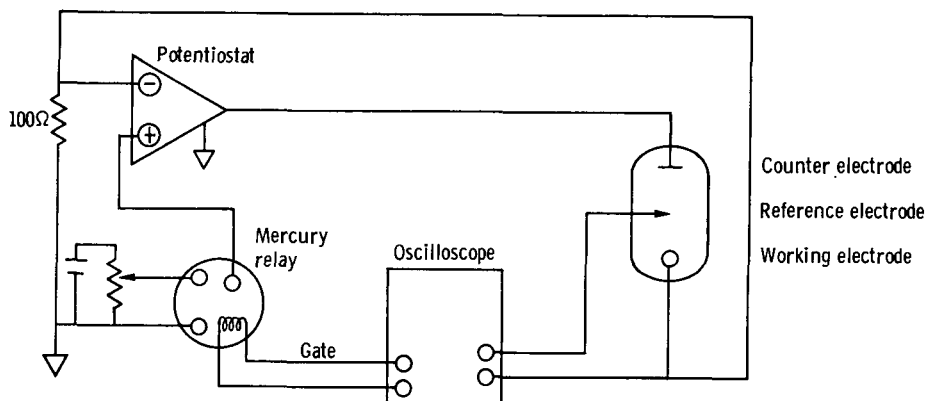
Figure 4. – Block diagram of circuit for galvanostatic measurements.

sis took place, thus minimizing electrode surface changes. It should be noted that the potential was not affected by concentration gradients since vigorous stirring (>100 rpm) had no effect on the magnitude of the potential, and that the 30-second, or steady, potential was only slightly higher than that observed in oscillographic traces recorded over a 10-second time interval. All steady-state potentials were corrected for the IR drop determined from the galvanostatic transient. The correction never exceeded 5 percent.

Preliminary Experiments

Experimental conditions considered initially included (1) the influence of the atmosphere within the cell (inert gas or vacuum) and (2) the magnitude of changes in the measured polarization curves with time. With respect to the former, vacuum-sealed cells and cells open to an excess pressure of dry nitrogen gas gave identical results. With respect to the latter, marked effects were observed. This is shown in figure 5, where the log of current density i against overpotential η is plotted (Tafel plot) for an electrode held at constant temperature and tested at various times up to 48 hours. The observed changes, no doubt, partly reflect roughening of the electrode surface. Since it is difficult to evaluate and correct for this kind of change, only freshly prepared cells were used for each series of runs reported, and the time period over which data were recorded never exceeded 3 hours from the time of filling the cell.
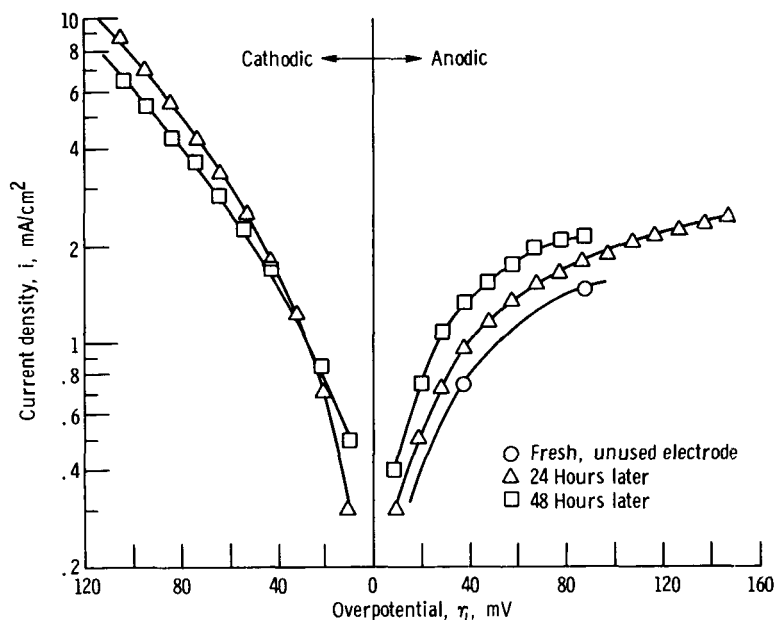
Figure 5. - Tafel plot for aluminum electrode in 50 mole percent AlCl$_3$ - 50 mole percent NaCl: time dependence. Temperature, 316° C (589 K).

Experimental Variables Considered

Table I lists the compositions of the electrolytes used and the temperatures and current density ranges over which measurements were made. All current densities are based on the apparent geometrical area of the electrode.

RESULTS AND DISCUSSION

The rate-determining process associated with electrochemical reactions can be explored by examining the current-voltage characteristics of the system. In electrochemical reactions, at least a part of the overpotential, defined as $\eta = E - E^O$ where E is the potential as current is being passed and E^O is the open-circuit potential, arises from a reaction in which ions and electrons are transferred across the double layer (i.e., "charge transfer"). Additional contributions may arise if (1) the rate of chemical reaction, or (2) the rate of mass transport to or from the electrode, or (3) the rate of adding or removing atoms from the crystal lattice are comparable to or slower than the rate of charge transfer. These effects give rise to chemical reaction overpotential, diffusion overpotential, and crystallization overpotential, respectively. These are thoroughly discussed by Vetter (ref. 12, p. 104)

If charge transfer is the rate-controlling step, the overpotential-current relation for anodic overpotentials $\gg RT/ZF$ is (ref. 12, p. 143)

$$\eta = \frac{-RT}{\alpha_a ZF} \ln i_o + \frac{RT}{\alpha_a ZF} \ln i_a \tag{1a}$$

and the overpotential at cathodic overpotentials $\gg RT/ZF$

$$\eta = \frac{RT}{\alpha_c ZF} \ln i_o - \frac{RT}{\alpha_c ZF} \ln i_c \tag{1b}$$

All symbols used are defined in the appendix.

The notation in equations (1) is modified from the reference cited in that the symbol for the cathodic transfer coefficient is changed from $1 - \alpha$ to α_c. The possibility that the cathodic transfer coefficient may not necessarily be equal to $1 - \alpha$ is discussed at length by Bauer (ref. 13).

Inspection of equations (1a) and (1b) indicates that a plot of η against $\ln i_a$ or $\ln i_c$ should result in a straight line with an intercept of $\ln i_o$ on the $\eta = 0$ axis. A linear $\log i$ against η plot (Tafel plot) is generally considered experimental evidence for a reaction in which the rate-determining step is the charge-transfer step. The slopes of the lines

$$\frac{\partial \eta}{\alpha \log i_a} = b_a = \frac{2.303\ RT}{\alpha_a ZF}$$

or

$$-\frac{\partial \eta}{\partial \log i_c} = -b_c = \frac{2.303\ RT}{\alpha_c ZF}$$

are called the anodic and cathodic Tafel slopes, respectively, and may be used for the calculation of the transfer coefficients α_a and α_c if the number of electrons transferred in the charge exchange rate-determining step Z is known. The apparent exchange currents $i_{o,c}$ and $i_{o,a}$ are obtained from the value of the respective intercepts at $\eta = 0$.

In addition to the study of current-potential characteristics, exploration of the transient time behavior of either current or potential in response to a potentiostatic or galvanostatic step perturbation provides greater insight into certain aspects of the rate-determining processes. This is particularly true for electrochemical dissolution and deposition reactions on solid electrodes encountered in the present work.

Mehl and Bockris (ref. 14) calculate that, if charge transfer alone were rate deter-

mining at low potentials $(\eta < RT/nF)$, the steady-state potential should be reached in a time t:

$$t = \frac{4RTC}{nFi_o} \tag{2}$$

where C is the double-layer capacity in microfarads per square centimeter. For a typical double-layer capacitance of 20 microfarads per square centimeter, n = 3, and $i_o = 10$ milliamperes per square centimeter, the steady-state potential should be reached in a time ≤ 150 microseconds. In addition, if charge transfer is rate controlling, a linear relation between η and time should only be observed for times necessary for the charging of the double layer (i.e., less than about 10^{-4} sec)(ref. 14). Mehl and Bockris (refs. 14 and 15), studying the dissolution and deposition of silver in aqueous perchlorate solutions, observed that the steady-state potential was reached in a time which was larger by a factor of 10 than that calculated from equation (2). In addition, the linearity between η and t extended for about 10^{-3} second. These effects were attributed to rate control at low overpotentials by diffusion of adions on the electrode surface.

Reddy (ref. 16) has reported similar effects for silver deposition in molten LiCl-KCl. Surface diffusion has also been noted for copper (refs. 17 and 18) and gallium (ref. 19) in aqueous solution.

Non-Steady-State Results

In this work, rise times to the steady state were observed which were in excess of 10 seconds at low current densities. This is much longer than the 150 microseconds calculated if charge transfer alone were involved (eq. (2)). The rise time decreased with increasing current densities. Figure 3 illustrates the potential rise for the first 180 milliseconds at a current density of 9.1 milliamperes per square centimeter in $AlCl_3 \cdot NaCl$ electrolyte. The potential-time data are shown in figure 2 for times up to 375 microseconds at a current density of 40 milliamperes per square centimeter. A linear relation is obtained for times which are longer than normally expected. A capacitance C calculated from the slope $\partial \eta / \partial t$ and current i in the equation

$$C = \frac{i}{\left(\dfrac{\partial \eta}{\partial t}\right)_{t \to 0}} = \frac{0.040 \times 10^{-3}}{0.104} = 385 \ \mu F/cm^2 \tag{3a}$$

is too large to be a double-layer capacitance, and is therefore apparently an adsorption

11

capacitance. The surface diffusion model described by Bockris and Damjanovic (ref. 20) allows the concentration of adsorbed species C_o to be estimated, using this potential-time data at low potentials, by means of the equations

$$C_o = \frac{RT}{n^2F^2} \frac{i}{\left(\frac{\partial \eta}{\partial t}\right)_{t \to 0}} \tag{3b}$$

$$C_o = \frac{RT}{n^2F^2} C \tag{3c}$$

Equations (3b) and (3c) are derived by assuming (1) a small coverage of the surface by adion and (2) a potential smaller than $RT/\alpha nF$. Table II lists the concentration of adions calculated for the aluminum anode in 50 mole percent $AlCl_3$ - 50 mole percent NaCl at 220° C (493 K) at various current densities. The average value is $(0.17\pm0.03)\times10^{-10}$ moles per square centimeter, which is the same order of magnitude as that reported for gallium in aqueous solution (ref. 19). Mehl and Bockris (ref. 15) report C_o values of 4×10^{-10} moles per square centimeter for silver in aqueous solution, and Reddy (ref. 16) reports $C_o = 9\times10^{-10}$ moles per square centimeter for silver in molten $(LiCl-KCl)_{eut}$.

An adion concentration of 0.18×10^{-10} moles per square centimeter corresponds to a surface coverage of only 0.001 if the radius of the adion is assumed to be the crystal radius of trivalent aluminum (0.5×10^{-8} cm, refs. 21 and 22).

The diffusion rate of adions on the surface nFv_o may be obtained provided the time

TABLE II. - CONCENTRATION OF ADIONS, SURFACE DIFFUSION

RATE, AND EXCHANGE CURRENT AS CALCULATED FROM

SURFACE DIFFUSION RATE FOR ALUMINUM ANODE IN

$AlCl_3 \cdot NaCl$ AT 220° C (493 K)

Current density, i, mA/cm^2	Concentration of adions, C_o, $moles/cm^2$	Surface diffusion rate, nFv_o, mA/cm^2	Calculated exchange current, $i_{o, calc}$, mA/cm^2
6.5	0.15×10^{-10}	3.7	1.52
8.5	.16	3.2	1.48
12.0	.15	3.7	1.72
25.5	.20	5.5	2.46
40.0	.19	5.7	2.66
Average	$0.17\pm0.03\times10^{-10}$	4.3 ± 1.4	1.97 ± 0.47

12

dependence of overpotential as it approaches the steady state is measured experimentally. The appropriate equation (ref. 20) is

$$nFv_0 = - \frac{d \ln(\eta_\infty - \eta)}{dt} nFC_0$$ (4)

Equation (4) can be evaluated from the adion concentration (table II) and the slope of a plot of $\log(\eta_\infty - \eta)$ against time. A typical plot is shown in figure 6. Values of η_∞ were obtained potentiostatically and are discussed further under Steady-State Results. Table II summarizes values of the surface diffusion rates obtained for aluminum anodes in $AlCl_3 \cdot NaCl$ at 220° C (493 K). As expected from the long rise times observed, the diffusion rates which average 0.0043 ampere per square centimeter are slower than those reported for silver either in aqueous solution (0.015 A/cm^2, ref. 15) or molten
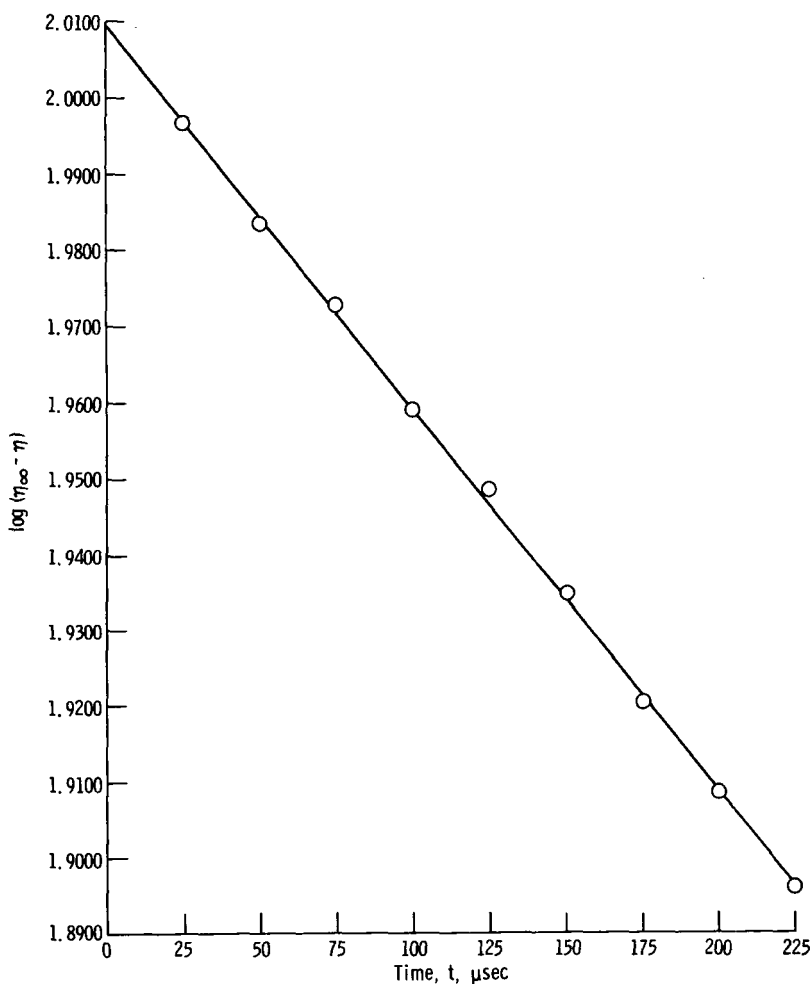

Figure 6. - Log $(\eta_\infty - \eta)$ as function of time. Electrolyte, $AlCl_3 \cdot NaCl$; current density, 40 milliamperes per square centimeter.

13

sàlts (3.3 A/cm^2, ref. 16). They are, however, larger than the value reported for the dissolution of gallium in aqueous solution at the same current density (0.0003 A/cm^2, ref. 19).

In their monograph, Bockris and Razumney (ref. 23, p. 41) indicate that the surface diffusion rate and the steady-state overpotential may be used to calculate an exchange current $i_{o,calc}$ which generally agrees with experimental exchange currents obtained from Tafel plots to within ±30 percent. Values of $i_{o,calc}$ obtained from the equation

$$\eta_{\infty} = -\left(\frac{RT}{nF} \frac{i}{i_{o,calc}} + \frac{RT}{\eta^2 F^2} \frac{i}{v_o} \right) \tag{5}$$

at various current densities i are also summarized in table II. The average value is 1.97 milliamperes per square centimeter, which agrees well with the experimental value of 1.88 milliamperes per square centimeter obtained from a Tafel plot.

All transient data discussed so far were taken in the 0- to 250-microsecond time period. Similar analyses of data in the 0- to 20-microsecond range gave smaller values for $i_{o,calc}$.

It appears then that the non-steady-state data for aluminum at low current densities (so that $\eta < RT/\alpha nF$) fit reasonably well into the surface diffusion model described by Bockris and coworkers. Aluminum in AlCl$_3 \cdot$NaCl melts appears to be quite similar to solid gallium in alkaline aqueous solutions as far as the surface diffusion parameters are concerned.

Bockris and Razumney (ref. 23, p. 33) conclude that probably all metals undergo deposition and dissolution at planar sites on the surface with subsequent diffusion along the surface to other sites. This is based on calculations of the heats of activation for transfer of silver ions to different kinds of sites on the surface: that is, planar surface, edge, kink, vacancy in an edge, and vacancy in a surface. The rate constant for transfer to a planar site is 10^6 times greater than to any other type of site. The rate-controlling process then becomes the diffusion of the adion on the surface either to or from this planar site. These same authors (ref. 23, p. 44) point out that there is a transition from surface diffusion control to another rate-controlling mechanism, such as charge transfer at higher current densities or overpotentials, and that a limiting current due to the surface diffusion occurs at still higher overpotentials.

Steady-State Results

Figure 7 is typical of the Tafel plots constructed from steady-state measurements. This particular plot is for aluminum in a 75 mole percent AlCl$_3$ - 25 mole percent
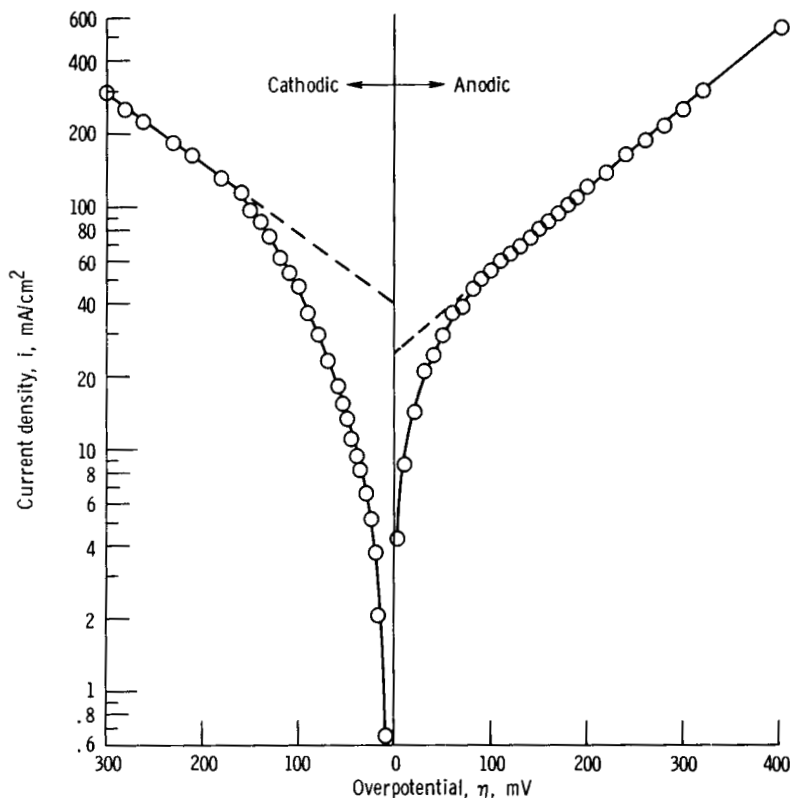
Figure 7. - Tafel plot for aluminum electrode in 75 mole percent $AlCl_3$ - 25 mole percent $(LiCl \cdot KCl)_{eut}$. Temperature, 235° C (508 K).

$(LiCl-KCl)_{eut}$ mixture at 235° C (508 K). A region of linearity is observed for both the anodic and cathodic branch extending from 80 millivolts on the anodic side and 170 milli-volts on the cathodic side.

The deviations from linearity are attributed partly to normal deviations from Tafel behavior caused by the increased importance of the back reaction at low overpotentials and partly by the surface diffusion effects already discussed. Since deviations from straight-line behavior resulting from the back reaction usually occur around 60 millivolts, the existence of surface diffusion effects is not evident from inspection of a Tafel plot such as figure 7. It is possible to construct a so-called Allen-Hickling plot (ref. 24) in which the function

$$Y = \log \frac{i}{1 - \exp\left(\dfrac{ZF\eta}{RT}\right)} \qquad (6)$$

is plotted against η. This gives a straight line over the entire potential range for reac-tions which are charge-transfer controlled over the entire potential range. Figure 8 is
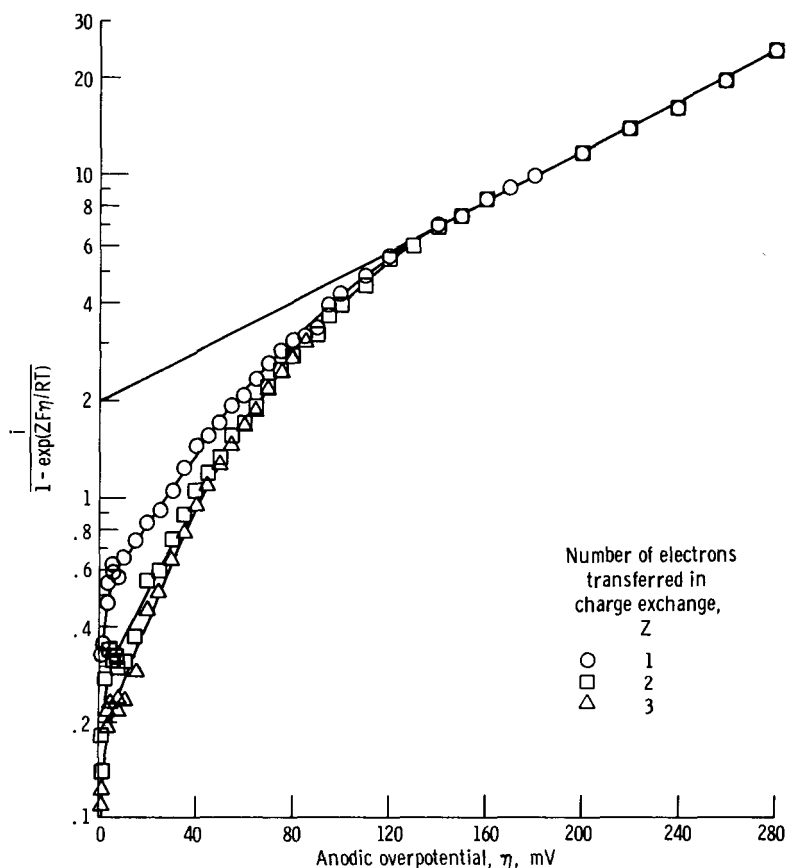
15

Figure 8. - Allen-Hickling plot for aluminum electrode in 67 mole percent AlCl$_3$ - 33 mole percent (LiCl-KCl)$_{eut}$. Temperature, 187° C (460 K).

such a plot for 67 percent AlCl$_3$ - 33 percent (LiCl-KCl)$_{eut}$ and clearly shows deviations from linearity in the low potential - low current region attributed to surface diffusion control of the reaction. Figure 8 shows equation (6) plotted for all possible values of Z, the number of electrons involved in the rate-determining step. No value of Z produces a straight line. It should be noted that the potential below which surface diffusion becomes rate determining is a function of the nature of the surface (ref. 25).

No evidence of a limiting current is found though potentials as high as ±350 millivolts were applied. In one experiment, however, the potential was increased to several volts in the anodic direction. An apparent limiting current of about 1 ampere per square centimeter was observed, the value of which did not oscillate with time or vary with the rate of stirring. This suggests a limiting current not caused by mass transport in the molten salt (ref. 26) but perhaps caused by chemical reaction or surface diffusion phenomena (ref. 25). This result is not conclusive, however, as the surface undergoes rapid changes at these high current densities.

The Tafel slopes in figure 7 are b_a = 2.3 RT/0.29 F and $-b_c$ = 2.3 RT/0.29 F, for

the anodic and cathodic reactions, respectively. The respective exchange currents are 26 and 39 milliamperes per square centimeter.

Results for the other temperatures and electrolytes studied are summarized in table III. The standard deviations obtained for all exchange currents and Tafel slopes were less than ±10 percent in most cases. While the uncertainty within one set of data was usually ±2 to ±3 percent, the reproducibility of one fresh cell to another varied as much as ±10 percent.

Note that the anodic exchange currents in table III range from a value of 1.3 milliamperes per square centimeter for the 50 mole percent $AlCl_3$ - 50 mole percent NaCl elec-

TABLE III. - SUMMARY OF TAFEL DATA

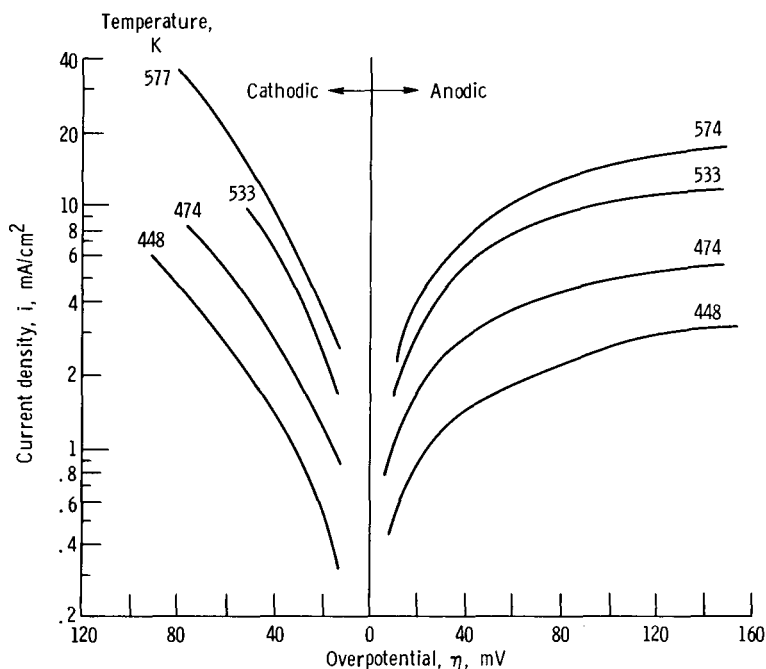| Electrolyte, mole percent	Temperature		Exchange current, mA/cm^2		Tafel slope		$E - E_{ref}$, mV
	^oC	K	Anodic	Cathodic	Anodic, b_a	Cathodic, b_c	
50 $AlCl_3$ - 50(LiCl-KCl)$_{eut}$	202	475	1.95±0.03	-	$\dfrac{2.303\ RT}{(0.304\pm0.005)F}$	-	<1
	213	486	2.93±0.05	-	$\dfrac{2.303\ RT}{(0.244\pm0.006)F}$	-	<1
67 $AlCl_3$ - 33(LiCl-KCl)$_{eut}$	187	460	1.92±0.02	9.6±0.5	$\dfrac{2.303\ RT}{(0.48\pm0.02)F}$	$\dfrac{2.303\ RT}{(0.40\pm0.01)F}$	275
75 $AlCl_3$ - 25(LiCl-KCl)$_{eut}$	235	508	31±2	39±3	$\dfrac{2.303\ RT}{(0.29\pm0.01)F}$	$\dfrac{2.303\ RT}{(0.29\pm0.02)F}$	400
	265	538	56±2	-	$\dfrac{2.303\ RT}{(0.27\pm0.03)F}$	-	-
50 $AlCl_3$ - 50 NaCl	175	448	1.3±0.1	0.9±0.4	$\dfrac{2.303\ RT}{(0.28\pm0.02)F}$	$\dfrac{2.303\ RT}{(1.0\pm0.3)F}$	-
	197	470	3.2±0.2	1.7±1.0	$\dfrac{2.303\ RT}{(0.20\pm0.02)F}$	$\dfrac{2.303\ RT}{(1.2\pm0.3)F}$	-
	253	526	7.9±0.4	3.4±0.1	$\dfrac{2.303\ RT}{(0.21\pm0.03)F}$	$\dfrac{2.303\ RT}{(1.23\pm0.03)F}$	-
	260	533	7.7±0.1	2.6±0.3	$\dfrac{2.303\ RT}{(0.18\pm0.01)F}$	$\dfrac{2.303\ RT}{(1.29\pm0.04)F}$	-
	304	577	9.3±0.4	4.3±0.4	$\dfrac{2.303\ RT}{(0.27\pm0.02)F}$	$\dfrac{2.303\ RT}{(1.39\pm0.06)F}$	-
	313	586	10.5±0.2	7.4±0.6	$\dfrac{2.303\ RT}{(0.24\pm0.01)F}$	$\dfrac{2.303\ RT}{(1.20\pm0.05)F}$	-

Figure 9. – Tafel plot for aluminum electrode in $AlCl_3 \cdot NaCl$: influence of temperature.

trolyte at 175° C (448 K) to a value of 56 milliamperes per square centimeter for the 75 mole percent $AlCl_3$ - 25 mole percent $(LiCl-KCl)_{eut}$ electrolyte at 265° C (538 K). For all $AlCl_3$-$(LiCl-KCl)_{eut}$ mixtures, the anodic and cathodic Tafel slopes are similar and vary with composition from about 2.3 RT/0.25 F to 2.3 RT/0.5 F. In contrast, for the $AlCl_3 \cdot NaCl$ electrolyte, the anodic slope is comparable to the others, but the cathodic slope is about a factor of 5 smaller.

The dependence of the overpotential - current density relation for aluminum in the $AlCl_3 \cdot NaCl$ mixture on temperature is shown in figure 9. It would have been instructive to compare the results for all the electrolytes at a common temperature. Unfortunately, attempts to use these observations to bring the data to a common "reduced" temperature based on the melting point proved unsuccessful.

The activation energies from a plot of $\log i_o$ against $1/T$ (fig. 10) for both the anodic and cathodic processes in the $AlCl_3 \cdot NaCl$ electrolyte are 7.3 ± 1.0 and 5.3 ± 0.6 kilocalories per mole (30.6 and 22.2 kJ/mole), respectively. These lie a little below the values of about 10 kilocalories per mole (41.9 kJ/mole) usually encountered (ref. 16).

In order to determine which processes are rate determining at high overpotentials (i.e., Tafel region), it is necessary to calculate Tafel slopes for various postulated sets of reactions and compare them with experiment. Fraser and Barradas (ref. 27) have described a simple method for carrying out these calculations. The anodic Tafel slope b_a is given by
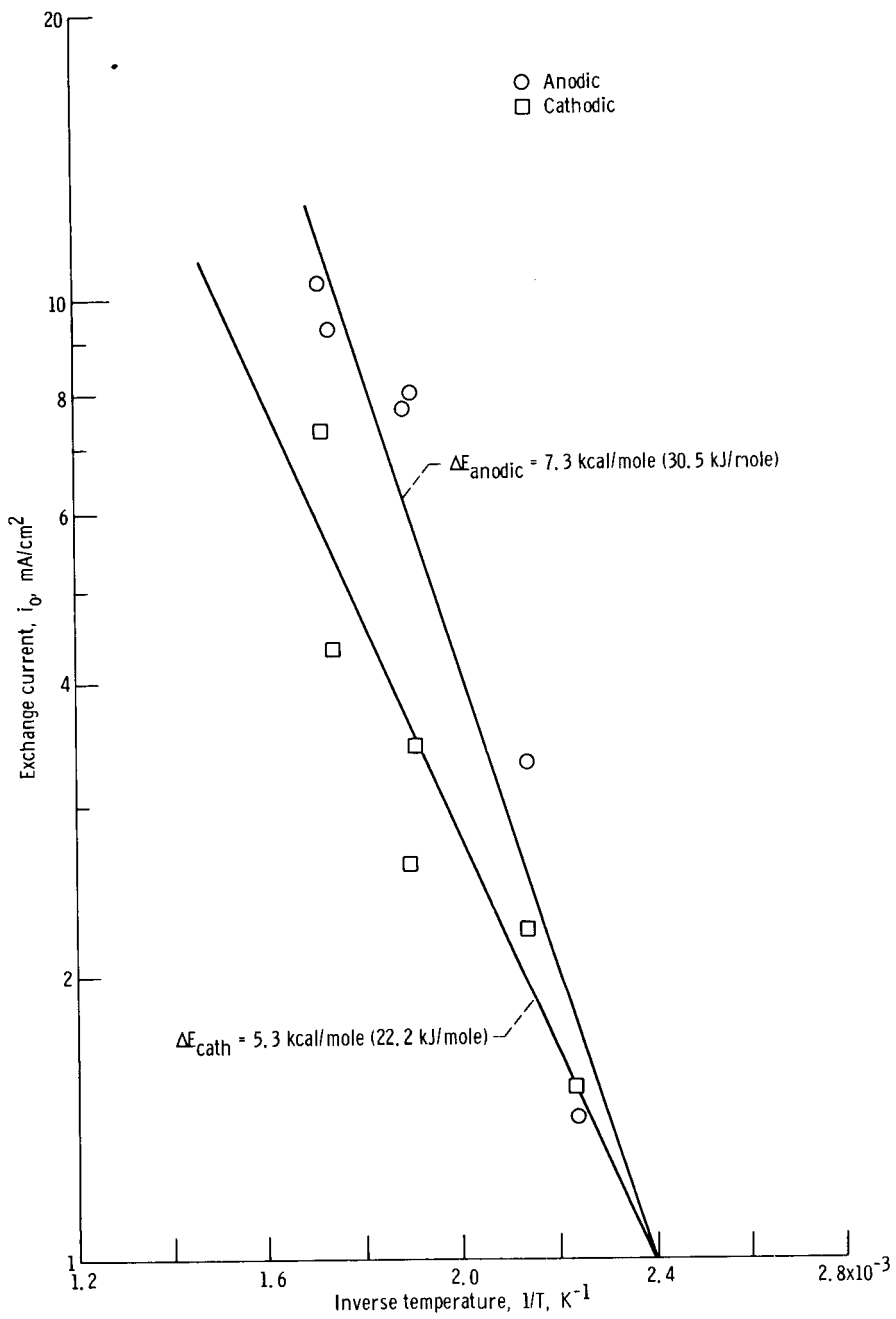
Figure 10. - Activation energy for charge-transfer process. Aluminum electrode in AlCl$_3$ · NaCl.
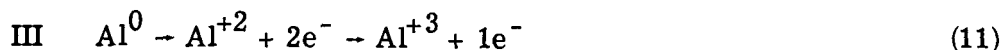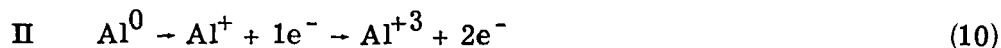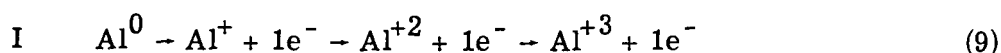
$$b_a = \frac{2.303 \; RT}{F} (\beta m - l)^{-1} \tag{7}$$

and the corresponding cathodic Tafel slope b_c is given by

$$b_c = - \frac{2.303 \; RT}{F} [k + (1 - \beta)m]^{-1} \tag{8}$$

where k, l, and m are the number of electrons involved in various stages of the overall reaction (see appendix).

The mechanisms chosen for analysis consisted of consecutive steps and did not consider the possibility of parallel processes. They are as follows, written for the anodic process:

$$\text{I} \qquad Al^0 \rightarrow Al^+ + 1e^- \rightarrow Al^{+2} + 1e^- \rightarrow Al^{+3} + 1e^- \tag{9}$$

$$\text{II} \qquad Al^0 \rightarrow Al^+ + 1e^- \rightarrow Al^{+3} + 2e^- \tag{10}$$

$$\text{III} \qquad Al^0 \rightarrow Al^{+2} + 2e^- \rightarrow Al^{+3} + 1e^- \tag{11}$$

$$\text{IV} \qquad Al^0 \rightarrow Al^{+3} + 3e^- \tag{12}$$

For the cathodic process the reactions are reversed. The use of simple bare-ion symbolism does not imply the absence of ligand coordination with Cl^- for example.

The calculated Tafel slopes for various rate-determining steps and the parameters used to compute them from equations (7) and (8) are presented in table IV. By comparing these expressions for the Tafel slopes with the experimental values in table III, it is possible to select the most probable rate-determining steps consistent with the data (table V).

For the anodic reaction in all electrolytes, the most probable rate-determining step is the one electron transfer constituting the first step in mechanisms I or II:

$$Al \rightarrow Al^+ + 1e^-$$

For this step, reasonable values of the true transfer coefficient β from 0.20 to 0.59 (table V) are obtained. The variation of β with composition should be noted. This implies structural changes, possibly, as the concentration of $AlCl_3$ is changed relative to the concentration and nature of the cations. Similar effects have been noted by Morrey (refs. 28 and 29) in spectroscopic studies in these media.

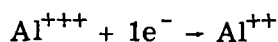For the cathodic reaction in the $AlCl_3$-$(LiCl-KCl)_{eut}$ mixtures, the most probable rate-determining step is

20

TABLE IV. - CALCULATED TAFEL SLOPES

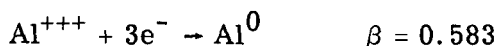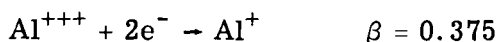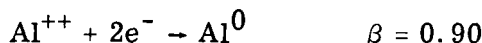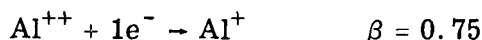| Mechanism	Rate-determining step (RDS)	Number of electrons involved in RDS, m	Number of electrons removed to permit RDS to occur once, l	Number of electrons which must be removed for products of RDS to be transferred to products, $-k$	Tafel slope	
					Anodic, b_a	Cathodic, $-b_c$
I, II	$Al^0 \rightarrow Al^+ + e^-$	1	0	2	$\dfrac{2.3\,RT}{\beta F}$	$\dfrac{2.3\,RT}{(3-\beta)F}$
I	$Al^+ \rightarrow Al^{+2} + e^-$	1	-1	1	$\dfrac{2.3\,RT}{(\beta+1)F}$	$\dfrac{2.3\,RT}{(2-\beta)F}$
I, III	$Al^{+2} \rightarrow Al^{+3} + e^-$	1	-2	0	$\dfrac{2.3\,RT}{(\beta+2)F}$	$\dfrac{2.3\,RT}{(1-\beta)F}$
III	$Al^0 \rightarrow Al^{+2} + 2e^-$	2	0	1	$\dfrac{2.3\,RT}{2\beta F}$	$\dfrac{2.3\,RT}{(3-2\beta)F}$
IV	$Al^0 \rightarrow Al^{+3} + 3e^-$	3	0	0	$\dfrac{2.3\,RT}{3\beta F}$	$\dfrac{2.3\,RT}{3(1-\beta)F}$
II	$Al^+ \rightarrow Al^{+3} + 2e^-$	2	-1	0	$\dfrac{2.3\,RT}{(2\beta+1)F}$	$\dfrac{2.3\,RT}{2(1-\beta)F}$

TABLE V. - MOST PROBABLE RATE-DETERMINING STEPS

FOR CHARGE-TRANSFER REACTION

Electrolyte, mole percent	Anodic rate-determining step	Anodic true transfer coefficient, β	Cathodic rate-determining step	Cathodic true transfer coefficient, β
50 $AlCl_3$ - 50 LiCl·KCl	$Al^0 \rightarrow Al^+ + e^-$	0.31	(a)	(a)
67 $AlCl_3$ - 33 LiCl·KCl	$Al^0 \rightarrow Al^+ + e^-$	.59	$Al^{+++} + e^- \rightarrow Al^{++}$	0.60
75 $AlCl_3$ - 25 LiCl·KCl	$Al^0 \rightarrow Al^+ + e^-$	.29	$Al^{+++} + e^- \rightarrow Al^{++}$	.71
50 $AlCl_3$ - 50 NaCl	$Al^0 \rightarrow Al^+ + e^-$	.20	$Al^{++} + e^- \rightarrow Al^+$	.75

[a]No analysis performed.

$$Al^{+++} + 1e^- \rightarrow Al^{++}$$

with true transfer coefficients β of 0.60 and 0.71. All other possibilities give values for β which are very close to 1 or larger. The cathodic reaction in the $AlCl_3 \cdot NaCl$ electrolyte clearly has a different rate-determining step than for the other solutions. Four possible rate-determining steps which give reasonable values for β are

$$Al^{++} + 1e^- \rightarrow Al^+ \qquad \beta = 0.75$$

$$Al^{++} + 2e^- \rightarrow Al^0 \qquad \beta = 0.90$$

$$Al^{+++} + 2e^- \rightarrow Al^+ \qquad \beta = 0.375$$

$$Al^{+++} + 3e^- \rightarrow Al^0 \qquad \beta = 0.583$$

The first of these reactions is proposed as the most probable rate-determining step since the activation energy for a multielectron transfer is very high (>100 kcal/mole, >418.6 kJ/mole) and therefore improbable (ref. 23, p. 36). It should be noted, though, that above $650°$ C (923 K) in fluoride melts, a three-electron transfer has been observed (ref. 30). The most probable rate-determining steps and the corresponding values for β are presented in table V.

That the rate-determining step for the cathodic reaction in the $AlCl_3$-$(LiCl$-$KCl)_{eut}$ melts is different from that in the $AlCl_3 \cdot NaCl$ melt is not surprising in view of recent Raman results on the structure of the $AlCl_4^-$ complex ion in $AlCl_3 \cdot KCl$ and $AlCl_3 \cdot NaCl$ melts (ref. 31). A regular tetrahedral symmetry T_d is found in the Na^+-containing melts, while a distorted tetrahedral (C_{2v}) symmetry is found in the K^+-containing melts. These structural differences could influence the relative rates of the steps in the reduction reaction.

In closing this discussion of the most probable rate-determining steps, it should be mentioned that a recent paper by Rangarajan (ref. 32) has criticized the analysis of Bockris and coworkers used in the present work. Very briefly, Rangarajan concludes that in cases where surface diffusion is rate limiting at low overpotentials, the Tafel slope at higher overpotentials is equal to twice the "true" slope (for change transfer) and the observed exchange current is larger than the true exchange current. The present results are not adequate to settle this theoretical dispute. In the present work, the Bockris treatment of surface diffusion has been employed since there is some evidence in the literature which experimentally supports it. The use of Rangarajan's equations would lead to other possible rate-determining steps. In addition, Rangarajan's treatment does not predict a limiting anodic current which was observed in at least one electrolyte in this study and has been observed by others for gallium (ref. 19). The Bockris approach predicts such a limiting current.

Current Efficiencies

Current efficiencies determined for aluminum anodes and cathodes in the $AlCl_3 \cdot NaCl$ melt by passing a known number of coulombs and measuring the weight loss of the anode and the weight gain of the cathode are summarized in table VI. The cathode efficiency could not be determined accurately because of the loss of some material during the repeated washings which were necessary to remove all traces of electrolyte from the elec-
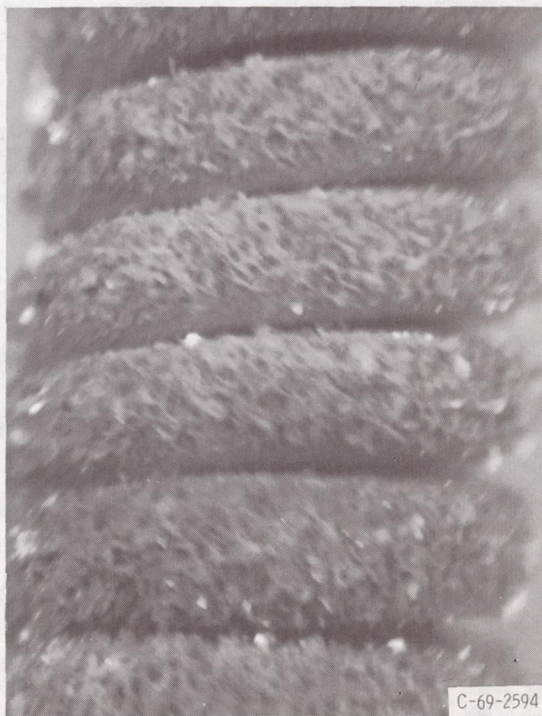
TABLE VI. - ANODIC AND CATHODIC EFFICIENCIES

OF Al IN LiCl· NaCl

Anodic		Cathodic	
Current density, mA/cm^2	Efficiency, percent	Current density, mA/cm^2	Efficiency, percent
0.3	100±1	0.1	>83
.5	98±2	.5	>62

(a) Anode. Electrolyzed at 0.3 milliampere per square centimeter.

(b) Cathode. Electrolyzed at 0.1 milliampere per square centimeter.

Figure 11. - Nature of electrode surface. X25.

trode. While the apparent inefficiency of the cathode is not considered to be real, it should be noted that these are preliminary results and further study is indicated.

Color photographs at 25 times enlargement were taken of both an anode and a cathode after electrolysis. The smooth surface of the anode with visible grain boundaries may be seen in figure 11(a). The crystallites of aluminum deposited on the cathode are seen in figure 11(b). These crystallites greatly increase the surface area. While some crystallites were mechanically removed during vigorous washing procedures, the deposit appears to adhere well enough to the surface that it would not create a problem in secondary cell applications. Very high current densities (10 A/cm^2) do produce a dendritic deposit and would not be suitable for use in a cell unless measures were taken to prevent such growth.

CONCLUSIONS

Aluminum appears to be a suitable negative electrode in a secondary battery when charged and discharged in alkali chloride - aluminum chloride molten salts at temperatures less than 250° C. The apparent exchange currents for discharge (dissolution) vary from about 2 to over 20 milliamperes per square centimeter as the concentration of AlCl$_3$ in the KCl-LiCl eutectic is increased from 50 mole percent to 75 mole percent. The apparent exchange currents for charging (deposition) vary from about 10 to 40 milliamperes per square centimeter over the same range of composition.

On the basis of an analysis of steady-state and transient overpotential data using the theoretical framework of Bockris et al., the following rate-determining steps for the anodic and cathodic reactions in the various electrolytes can be proposed:

1. At low overpotentials, less than 70 millivolts anodic and 170 millivolts cathodic, the rate-determining step is the diffusion of adions on the metal surface. The concentration of adions was found to be 0.2×10^{-10} moles per square centimeter and the surface diffusion velocity 0.0043 ampere per square centimeter in AlCl$_3 \cdot$ NaCl melts.

2. At higher overpotentials the rate-determining steps are charge transfer. In the anodic reaction, for all electrolytes, the most probable rate-determining step is $Al \rightarrow Al^+ + e^-$. For the cathodic reaction, the most probable rate-determining step is $Al^{+++} + e^- \rightarrow Al^{++}$ in the AlCl$_3$-(KCl-LiCl) eutectic mixtures and $Al^{++} + e^- \rightarrow Al^+$ in the AlCl$_3 \cdot$ NaCl melts.

These conclusions about the charge-transfer steps cannot be considered unambiguous as they are deduced from a consideration of Tafel data and are based on the assumption that the true transfer coefficient should be between 0.20 and 0.80 and that one-electron transfers are most probable.

Current efficiencies for dissolution were close to 100 percent at current densities up to 0.5 milliampere per square centimeter. The measurements were inaccurate for deposition, but a strong adherent deposit was obtained at low current density. Dendrites were observed at current densities larger than 10 milliamperes per square centimeter.

Lewis Research Center,
  National Aeronautics and Space Administration,
    Cleveland, Ohio, August 8, 1969,
      120-34.

APPENDIX - SYMBOLS

b   Tafel slope, mV

C   double-layer capacitance, $\mu F/cm^2$

C_o concentration of adions, $moles/cm^2$

F   faraday, 96 500 C

i   current density (anodic+, cathodic-), mA/cm^2

i_o apparent exchange current, mA/cm^2

-k   number of electrons which must be removed to permit products of rate-determining step to be transferred to products

l number of electrons which must be removed to permit rate-determining step to occur once

m   number of electrons involved in rate-determining step

n   number of electrons transferred in overall reaction

nFv_o surface diffusion velocity, mA/cm^2

R   gas constant, 8.314 VC/mole deg

T   temperature, K

t   time, sec

v_o surface diffusion flux, $mole/(cm^2)(sec)$

Z   number of electrons transferred in charge-exchange rate-determining step

α anodic, cathodic apparent transfer coefficient

β true transfer coefficient

η overpotential (anodic +, cathodic -), mV

η_∞ steady-state overpotential

Subscripts:

a   anodic

c   cathodic

calc   calculated

REFERENCES

1. Zaromb, S.: Aluminum Fuel Cells for Electric Vehicles. Power Systems for Electric Vehicles Symposium, U.S. Dept. of Health, Education, and Welfare, Apr. 6-8, 1967.

2. Brenner, Abner: Electrolysis of Organic Solvents with Reference to the Electrodeposition of Metals. J. Electrochem. Soc., vol. 106, no. 2, Feb. 1959, pp. 148-154.

3. Edwards, Junius D.; Taylor, Cyrie S.; Cosgrove, Lee A.; and Russell, Allen S.: Electrical Conductivity and Density of Molten Cryolite with Additives. J. Electrochem. Soc., vol. 100, 1953, pp. 508-512.

4. Yamaguti, Yohei; and Sisido, Syunsuke: The Electrolytic Conduction of Fused Salts. II. J. Chem. Soc. Japan, vol. 62, 1941, pp. 304-307.

5. Frank, William B.; and Foster, L. M.: Investigation of Transport Phenomena in the Cryolite-Alumina System by Means of Radioactive Tracers. J. Phys. Chem., vol. 61, no. 11, Nov. 1957, pp. 1531-1536.

6. Haupin, Warren E.: Metal Mists and Aluminum Losses in the Hall Process. J. Electrochem. Soc., vol. 107, no. 3, Mar. 1960, pp. 232-236.

7. Laitinen, H. A.; and Liu, C. H.: An Electromotive Force Series in Molten Lithium Chloride - Potassium Chloride Eutectic. J. Am. Chem. Soc., vol. 80, no. 5, Mar. 12, 1958, pp. 1015-1020.

8. Piontelli, R.: Research on Anodic and Cathodic Behavior of Metals. Tech. Note 7, Politecnico di Milano, Laboratoris di Elettrochimica, Italy (OSR TN 56-546), Sept. 1956.

9. King, L. A.; Brown, A. D., Jr.; and Frayer, F. H.: High Energy Density Electrochemical Cells. Proceedings of the 1968 OAR Research Applications Conference, vol. 1, Rep. OAR-68-001, Institute for Defense Analyses, Mar. 21, 1968. (Available from DDC as AD-666800.)

10. Munday, Theodore C. F.; and Corbett, John D.: An Electromotive Force Study of Lower Oxidation States of Lead, Cadmium, and Tin in Molten $NaAlCl_4$. Inorg. Chem., vol. 5, no. 7, July 1966, pp. 1263-1268.

11. Giner, José; and Burrows, Brian: Aluminum Chlorine Battery. Tyco Labs, Inc. (NASA CR-100 763), Oct. 1968.

12. Vetter, Klaus J.: Electrochemical Kinetics: Theoretical and Experimental Aspects. Academic Press, 1967.

13. Bauer, Henry H.: The Electrochemical Transfer Coefficient. J. Electroanal. Chem., vol. 16, no. 3, 1968, pp. 419-432.

14. Mehl, Wolfgang; and Bockris, John O'M.: On the Mechanism of Electrolytic Deposition and Dissolution of Silver. Can. J. Chem., vol. 37, no. 1, Jan. 1959, pp. 190-204.

15. Mehl, W.; and Bockris, J. O'M.: Mechanism of Electrolytic Silver Deposition and Dissolution. J. Chem. Phys., vol. 27, no. 3, Sept. 1957, pp. 818-819.

16. Reddy, Thomas B.: Surface Diffusion Processes and Dendritic Growth in the Electrodeposition of Silver from Molten Halides. J. Electrochem. Soc., vol. 113, no. 2, Feb. 1966, pp. 117-123.

17. Bockris, J. O'M.; and Enyo, M.: Mechanism of Electrodeposition and Dissolution Processes of Copper in Aqueous Solutions. Trans. Faraday Soc., vol. 58, 1963, pp. 1187-1202.

18. Mattsson, E.; and Bockris, J. O'M.: Galvanostatic Studies on the Kinetics of Deposition and Dissolution in the Copper + Copper Sulphate System. Trans. Faraday Soc., vol. 55, 1959, pp. 1586-1601.

19. Bockris, J. O'M.; and Enyo, M.: Electrodeposition of Gallium on Liquid and Solid Gallium Electrodes in Alkaline Solutions. J. Electrochem. Soc., vol. 109, no. 1, Jan. 1962, pp. 48-54.

20. Bockris, J. O'M.; and Damjanovic, A.: The Mechanism of the Electrodeposition of Metals. Modern Aspects of Electrochemistry, vol. 3, J. O'M. Bockris and B. E. Conway, eds., Butterworth Publ., 1964, pp. 224-346.

21. Pauling, Linus C.: The Nature of the Chemical Bond and the Structure of Molecules and Crystals. Second ed., Cornell Univ. Press, 1940, p. 346.

22. Moeller, Therald: Inorganic Chemistry. John Wiley & Sons, Inc., 1952, p. 734.

23. Bockris, J. O'M.; and Razumney, G. A.: Fundamental Aspects of Electrocrystallization. Plenum Press, 1967.

24. Delahay, Paul: Double Layer and Electrode Kinetics. Interscience Publ., 1965, p. 163.

25. Damjanovic, A.; and Bockris, J. O'M.: The Kinetics of the Electrodeposition and Dissolution of Metal Monolayers as a Function of Dislocation Density. J. Electrochem. Soc., vol. 110, no. 10, Oct. 1963, pp. 1035-1044.

26. Vetter, K. J.: Electrochemical Kinetics: Theoretical and Experimental Aspects. Academic Press, 1967, p. 400.

27. Fraser, G. H.: and Barradas, R. G.: A Simplified Calculation of Tafel Slopes for Successive Electrochemical Reactions. J. Electrochem. Soc., vol. 112, no. 4, Apr. 1965, pp. 462-464.

28. Morrey, John R.: Fused Salt Spectrophotometry. IV. Uranium (IV) in Chloride Melts. Inorg. Chem., vol. 2, no. 1, Feb. 1963, pp. 163-169.

29. Morrey, J. R.; and Voiland, E. E.: High-Temperature Absorption Spectrophotometry. II. The Effect of Black-Body and Sample Emission on Absorption Spectra. Spectrochim. Acta, vol. 18, 1962, pp. 1175-1186.

30. Senderoff, S.; and Mellors, G. W.: The Electrodeposition of Coherent Deposits of Refractory Metals. IV. The Electrode Reactions in the Deposition of Niobium. J. Electrochem. Soc., vol. 113, no. 1, Jan. 1966, pp. 66-71.

31. Balasubrahmanyam, K.; and Nanis, L.: Raman Spectra of Liquid $AlCl_3 \cdot KCl$ and $AlCl_3 \cdot NaCl$. J. Chem. Phys., vol. 42, no. 2, Jan. 15, 1965, pp. 676-680.

32. Rangarajan, S. K.: Surface Diffusion and Galvanostatic Transients. I. J. Electroanal. Chem., vol. 16, no. 4, Apr. 1968, pp. 485-492.